

THE SYNTHETIC HAZE SIMULATION BASED ON VISIBILITY RANGE FOR DEHAZING METHOD IN SINGLE IMAGE

¹SARUDIN KARI, ²NOOR ASMA HUSAIN, ³ABDULLAH BADE, ⁴MOHD SHAFRY MOHD RAHIM

^{1,3}Faculty of Science and Natural Resources, Universiti Malaysia Sabah

^{2,4}School of Computing, Faculty of Engineering, Universiti Teknologi Malaysia

E-mail: ¹sarudin@ums.edu.my, ²asma4@live.utm.my, ³abb@ums.edu.my, ⁴shafry@utm.my

ABSTRACT

Outdoor images are typically degraded by light scattering and absorption from aerosols, such as dust, mist, and smoke in the atmosphere. Because of poor visibility, dimmed brightness, low contrast, and colour distortion, these phenomena affect the captured image. Therefore, it is a critical challenge to recover pictures taken in a haze condition, which is called image dehazing. The primary aim of image dehazing is to improve details on visibility, edge, and texture and retain the image structure and colours without data loss. There are no proven benchmarks for their assessment, despite the many algorithms suggested for single image dehazing. In previous publications, arbitrary comparisons were mostly focused on a small number of images, with different publications using different sets of images. This paper presents a new dataset that includes image pairs of hazy and corresponding outdoor images that are haze-free (ground-truth). Most of the current hazy database presented in a single image simulated synthetic haze indicated complicated calculation of the depth map. Unlike most of the current dehazing databases, a synthetic haze, which is determined by the atmospheric scattering algorithm derived from the actual distance from the camera to the scene object, has simulated hazy images. In the separate range, the synthetic haze derivation referred from the meteorological range explicitly based on haze conditions. On a clear day as referred to as a low Air Pollutant Index, this experiment simulated synthetic haze in the Malaysian outdoor scene. The haze simulation illustrates how this approach can lead to better outcomes in the measurement of image quality than the current state-of-the-art dehazing method.

Keywords: *Haze, atmospheric scattering model, dehazing, synthetic haze*

1. INTRODUCTION

The atmospheric phenomena of smoke, fog, and mist are all attributed to contaminants such as dust, sand, water droplets, or ice crystals from the atmosphere. These phenomena in meteorology mainly vary due to material, scale, shape, and concentration. Their physical effects on imagery, however, are identical. Haze consists of an aerosol, a distributed system of small particles that are suspended in the air or gas. Haze has a wide range of origins, including volcanic ashes, exudation of leaves, combustion products, and sea salt. Haze appears to create a distinctive hue of grey or bluish and affects visibility [1]. Haze is a deterioration found in outdoor images, especially for computer vision applications, where image contrast is decreased as particles suspended in the air disperse the light. This condition induces low contrast and

poor picture visibility. The loss of detail caused by haze makes images visually unappealing and poses challenges for both human and machine vision, making it difficult to recognize, track objects or navigate [2,3]. This research involves image processing research area, especially in image restoration. Most of the image restoration overcomes blurring, noise and misfocusing in certain images. However, in this research, the focus is on image dehazing approach which focuses on removing haze effectively.

To clarify haze, Koschmieder suggested a physical model in which horizontal airlight dispersion and reflection and propagation-based attenuation led to the image's low quality [4]. Their contributions are determined by the media's optical thickness between the camera's sensor and the object being captured. The direct transmission from the

scene to the camera is decreased by scattering and absorption, introducing another layer of the ambient scattered light, known as airlight, as shown in Figure 1.

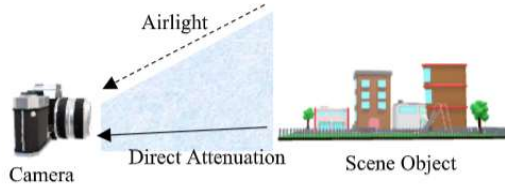


Figure 1: Scattering phenomena

The attenuated direct transmission causes the scene to be lower in intensity, and the airlight causes the presence of the scene to be blurred out. There has been significant improvement in previous studies in approaches that use images captured in hazy scenes. Atmospheric signals are used by Cozman and Krotkov [5] and Nayar and Narasimhan [1] to estimate depth. Since then, many explicit visibility enhancement methods have been implemented, which can be grouped into four categories: multi-image methods [6], filter-based polarization methods [7], methods using proven depth or geometry [8], and single-image methods [9-19].

Most of the single image dehazing algorithms have recently implemented different approaches to restore the haze image to become a natural haze-free image. Both techniques were built on a similar principle; to recover the haze from the clean scene. Estimating an accurate medium for the transmission map is essential. With Tan [9] and Fattal [10], a breakthrough was made in enhancing single-image visibility that can automatically dehaze a single image without additional details, such as established geometrical information or user feedback. The existence of halos around depth discontinuity due to the local window-based operation is one of the process's disadvantages. Tan's early work provides a less accurate calculation. In certain other instances, Fattal is not stable, and it obtains an accurate estimation when obtaining the most massive error. Fattal works well only at low levels of haze, and at medium and high levels of haze, the output decreases. Fattal proposes a different approach based on colour lines, but with low luminosity [11]. Tarel and Hautiere [12-13] introduce a rapid restoration of visibility whose complexity is linear to the number of pixels of the image. He found that most outdoor items have at least one colour channel that is substantially dark in clear weather [14-15]. Computation time is one of

the disadvantages of the techniques. For real-time applications, where the input scenes' depths shift from frame to frame, the methods cannot be implemented. Before evaluating the initial transmission values by adding its lower bound, Meng [16] extends the dark channel's concept. He and Meng also slightly underestimate the transmission of the two techniques since they effectively predict the lower bound of transmission. When the haze level rises, the calculation of He and Meng becomes more precise. Ancuti suggests a process based on image fusion, but it distorts colour [19]. Tang provides a framework focused on learning. The technique collects multi-scale characteristics such as dark channel [17], maximum local contrast, hue disparity, and maximum local saturation. It uses the random forest regressor to learn the association between the characteristics and the transmission, Cai [20] proposes a Tang-like learning system that trains a regressor to predict the transmission value from its surrounding patch. However, with a correct atmospheric light colour, the learning-based techniques rely heavily on the white balance step. Once there are minor errors in the measurement of ambient light colour, their output drops rapidly. Berman [21] suggests an algorithm based on a previous modern non-local one. At a medium haze level, Berman can achieve the least transmission estimation error, but the error increases at both low and heavy haze levels.

Earlier research explores the issues detected on managing haze at various levels. Some of the approaches did not cater to a dense haze level, and some of the approaches did not cater to low haze level [11,19,21]. Thus, it shows the importance of image dehazing assessment at a variety of haze levels. A volume of a dataset is required to fulfil this requirement in order to assess the efficiency of image dehazing method to dehaze at all haze levels.

Table 1: Center Table Captions Above the Tables.

Year	Method	Scene	Depth-based
2012	FRIDA	Outdoor	Free-Space Segmentation (FSS)
2016	DHAZY	Indoor	Stereo image
2016	CHIC	Indoor	Actual Distance
2017	HAZERD	Outdoor	fusing structure from motion and lidar [26]
2018	IHAZY	Indoor	Stereo images
2018	OHAZY	Outdoor	Stereo images
2019	VHAZE*	Outdoor	Actual distance

*our dataset

However, there are not enough proven criteria or benchmarks for their assessment in managing various haze levels [11,19,21], despite many algorithms suggested for single image dehazing.

In previous work, six datasets: FRIDA [13], D-hazy [22], CHIC [23], HAZERD [24], O-HAZY [25], and I-HAZY [26] were proposed for objective algorithm evaluation, as shown in Table 1. FRIDA is very specialized and offers a driver's point of view with many synthetic hazy road images. Indoor scenes that are not indicative of a traditional dehazing program, D-hazy uses depth images from Middlebury [27] and NYU depth V2 [28]. In an indoor setting, CHIC utilizes a fog machine and provides two indoor scenes with known objects and two scenes that include window-viewed outdoor content. A new VHAZE image dataset, known as Visibility Haze Simulation, has been proposed in this paper, which has simulated synthetic haze with four different levels based on visibility range as in Table 4. The visibility ranges were referred to weather conditions could be benchmarking assessment for future image dehazing.

2. HAZE IMAGING MODEL

In the atmospheric scattering model, it has two mechanisms which are direct attenuation, $J(x)t(x)$ and airlight, $A(1 - t(x))$ as illustrated in Figure 1. Haze algorithm combined these mechanisms, given by [4], as follows:

$$I(x) = J(x)t(x) + A(1 - t(x)) \quad (1)$$

where $I(x)$ represent haze image, $J(x)$ represents a haze-free image, $t(x)$ represents direct transmission, and A is the airlight.

2.1 Airlight

In addition to the light from the source (or reflected objects) that passes through the medium and is transmitted to the camera, the ambient illumination in the atmosphere is also dispersed by the same particles towards the camera.

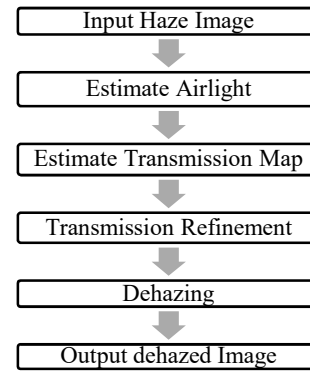


Figure 2: The process flow of the dehazing framework

The most haze-opaque pixel was used for the measurement of air-light in early works. Tan selected the brightest pixel [9]. Fattal [10] used it for an optimization problem as an initial guess. However, rather than air-light, the pixel with the highest intensity might correspond to a bright object. He recommends choosing the brightest pixel among the pixels with the dark channel's top brightest values (the minimal colour channel in a small environment) [14]. This approach is practical and usually produces precise results, but it assumes that the sky or another region is visible in the picture with no objects in line-of-sight. Tarel and Hauti'ere carry out White-balance, and pure white (1, 1, 1) [12] is believed to be the air-light in RGB value. Sulami et al. [29] estimate the magnitude and direction of air-light separately. By searching for small patches with continuous transmission and surface albedo, the path is estimated. This way is used by Bahat and Irani [30] until variations between co-occurring patches are identified, and air-light measured. Both methods [29, 30] require pairs of patches that meet certain conditions to be identified. Such systems are computer-intensive. To estimate the air-light [31], Berman uses a Hough transform. Hough transform is a useful technique via a voting scheme to detect unknown parameters of a model given noisy data.

2.2 Transmission Map

The most challenging part is the calculation of transmission maps $t(x)$ between the radiance of the camera and the scene. The distance $d(x)$ from the camera observer is the point of a scene. The transmission of haze is found to be physically linked to depth. Depth estimation is an essential but challenging issue in computer vision [14].

$$t(x) = e^{-\beta d(x)} \quad (2)$$

Direct transmission is formulated by the atmospheric dispersion coefficient, β , the distance or

depth of the scene, d , between the observer and the target object [32]. It is worth noting that the most important information is the depth of the scene. Since the scattering coefficient, β , can be considered a constant homogeneous atmospheric condition, if the depth is given, the medium transmission $t(x)$ can easily be calculated according to Equation (2). $T(x)$ represents a transmission map in the scalar $[0,1]$. Incorrect estimation of the transmission diagram, such as false textures and halo artefacts, can lead to issues. For this reason, several approaches to further refinement of transmission have been established. The method of smoothing used to improve the accuracy of the transmission map varies from many dehazing techniques. Gaussian, bilateral, soft matting, and guided filter are some of the filtering approaches used. In the final scene, radiance $J(x)$ is determined by using Equation (3) as given by Koshmieder [4] after the atmospheric light, and the transmission map are obtained:

$$J(x) = \frac{I(x) - A}{t(x)} + A \quad (3)$$

Equation 3 shows the reverse algorithm from Equation 1 to restore a haze image based on transmission and airlight estimation. This formula was used for most dehazing processes and included in our methodology, which will be explained in the next section.

3. METHODOLOGY

This segment clarified our haze simulation methodology. The entire system demonstrates that our Visibility Range of Haze Simulation algorithm includes the whole dehazing method process. Figure 3 is a summary of the flow of processes from the development of the dataset to the dehazing assessment. The haze simulation is determined using the model of atmospheric scattering in Equation (1):

$$I(x) = J(x)t(x) + A(1 - t(x)). \quad (1)$$

To get a haze image, $I(x)$, requires a haze-free image, $J(x)$, airlight value, A and transmission value, $t(x)$. The default RGB value of an airlight is set to $[1,1,1]$. A clear image with a known distance $d(x)$ between the camera and the target is captured. The scattering coefficient, β derived based on the captured distance map. Then it will calculate the transmission map value as in Equation (2). Based on the air pollutant index and environmental conditions, the picture taken must be on a clear day to be classified as a haze-free image. The synthetic haze was only simulated in a clear picture, according to

the meteorological range [32]. The simulation creates four different haze conditions in a haze-free image.

Five dehazing techniques have been applied to these haze conditions to remove haze in a precise way. The dehazed image was then assessed by using image quality measurement and benchmarking against the haze-free image.

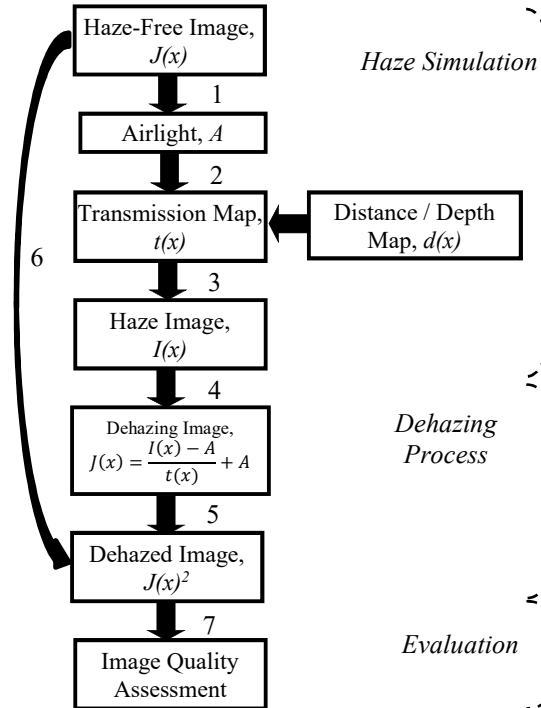


Figure 3: The diagram of haze simulation

This experimental for haze simulation has been set up and coded using MATLAB 2017b with a CPU (Intel i5 7200, 2.5GHz 8GB). This standard process obtained and referred from the previous research made by Zhang [24].

4. HAZE SIMULATION

With image quality evaluation, the synthetic haze image will be used to assess the quality of the process. The optimum value of the image quality measurement between the initial image and the dehaze image must be obtained. It can also be an added advantage and assist in creating a haze-free picture of quality. Therefore, with haze simulation, we suggest a new dataset. A clear picture taken on a clear day of the outdoor scene in Malaysia that takes the weather into account is good, and the air pollutant index is in a Good category. An

example of one of the captured image properties for the VHAZE dataset is as follows:

Table 2: The Properties of Haze-Free Dataset

Venue	UTM KL Entrance
Time	Monday, 12 March 2018 1:18 PM
API	22 – Good
Temperature	31°C - Clouds and Sun
Distance	200 meters
Device	Canon EOS 5D Mark III, Lens 17 mm
Dimensions	864 x 576 pixels
Image Type	PNG
Properties	ISO 250, Aperture f/4, Shutter Speed 1/1000 sec

It displays the properties of one of the VHAZE datasets, based on Table 2. The air pollutant index reading is 22, which means that it is in a Good category. The temperature reading is 31°C, which is a condition to show that it is a clear day. An API value of 0 to 50, based on Table 3, means good air quality with minimal potential for public and environmental health effects. The API value of 300-500, on the other hand, is a risky air quality with a more significant potential environmental and public health effect. An Air Pollutant Index (API) is a number used to convey the polluted air or the forecast by government agencies. The concentration of each pollutant varies; API values are therefore grouped into ranges allocated to a standardized public health warning [33].

Table 3: Air Pollutant Index Category

CATEGORY	AIR POLLUTANT INDEX	VISIBILITY RANGE (M)	VISIBILITY RANGE (KM)
GOOD	0-50	>10	>16.1
MODERATE	51-100	5-10	8.05-16.1
UNHEALTHY FOR SENSITIVE GROUP	101-150	3-5	4.83-8.05
UNHEALTHY	151-200	1.5-3	2.41-4.83
VERY UNHEALTHY	201-300	1	1.61-4.83
HAZARDOUS	300 >	<1	<1.61

These properties' values simulate the hazy images and the captured haze-free image with a distance $d(x)$, calculated in kilometres (km) by Distance Calculator application as in Figure 4.

The dehazing method's efficiency can be proved with several haze level conditions provided by Zhang [24]. Zhang simulates five different conditions, from light to dense fog. The scattering

parameter β depends on the weather condition. Specifically, this scattering parameter is obtained from the visible range, R_m via the relation $\beta = \frac{-\ln(\epsilon)}{R_m}$ [32]. These parameters are used to simulate the hazy images and a captured haze-free image with an associated depth map $d(x,y)$, as shown in Figure 5. The contrast threshold ϵ is set as 0.02. The haze ranges from 1 kilometre to 10 kilometres have been referred to simulate synthetic haze [24]. In this paper, four different conditions have been used, which consists of 1km, 2km, 3km, and 4km, as listed in Table 4.

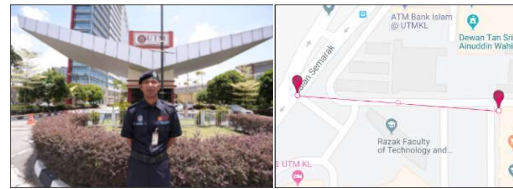


Figure 4: The captured clear image and distance measurement with the Distance Calculator application.

Table 4: The Weather Conditions Visibility Range and Its Scattering Coefficient [32]

No.	Weather Condition	Visibility Range, km	Scattering Coefficient, β
1	Dense Fog	< 50 m	>78.2
2	Thick Fog	50 m – 200 m	78.2 – 19.6
3	Moderate Fog	200 m – 500 m	19.6 – 7.82
4	Light Fog	500 m – 1000 m	7.82 – 3.91
5	Thin Fog / Dense Haze	1 km – 2 km	3.91 – 1.96
6	Haze	2 km – 4 km	1.96 – 0.954
7	Light Haze	4 km – 10 km	0.954 – 0.391
8	Clear	10 km – 20 km	0.391 – 0.196
9	Very Clear	20 km – 50 km	0.196 – 0.078
10	Exceptionally Clear	>50 km	0.078
11	Pure Air	277 km	0.0141



Figure 5: The depth map from Zhang method [24].

The process of haze simulation summarized as follow:

The proposed VHaze Simulation Algorithm

BEGIN: Input haze-free image: $J(x)$

Step 1: Define default airlight value, $A = [1,1,1]$

Step 2: Define default beta parameter $\beta = 3.912$

Step 3: Define a transmission map, $t(x)$

Step 4: Measure scene depth, $d(x)$ with Distance Calculator

for each haze visibility range, R_m [1,2,3,4] in kilometre

Step 4.1: define the scattering coefficient,

$$\beta = \frac{3.912}{R_m}$$

Step 4.2: calculate the transmission value, $t(x) = e^{-\beta d(x)}$

Step 4.3: calculate $I(x) = J(x)t(x) + A(1-t(x))$

end
END: Output hazy image: $I(x)$

Based on the dataset properties in Table 2, we simulate the synthetic haze into four categories according to haze weather conditions in Table 3. To define the transmission map as Equation (2), we have the actual distance (in kilometres) for the scene and calculate the transmission as Step 4.2:

$$t(x) = e^{-\beta d(x)}$$

For example,

for 1 kilometre,

$$t(x) = e^{-(3.91)(0.2)} = 0.457$$

for 2 kilometres,

$$t(x_{|\beta=1.96|}) = e^{-(1.96)(0.2)} = 0.676$$

Once we get the transmission value, the next step is Step 4.3, to execute the hazy image by using Equation (1). This research also used an auxiliary structure provided from Zhang [22] that associated the ground truth depth map derived by using fusing structure from motion and lidar [34]. From the ground truth depth map, the synthetic haze is applied to simulated the original image into four haze conditions $t(x_{|\beta=1,2,3,4|})$. Therefore, this experiment is applied in two ways for haze simulation, using the actual distance map and a ground truth depth map.








5. HAZE DATASET

This section shows the result of our simulation of synthetic haze to a single image. It consists of two different depth information, which used actual distance map and ground truth depth map. Both datasets have been simulated into four hazy conditions as in Table 5. In Table V; these datasets will become an input to the dehazing method. The difference of hazy conditions can be seen at each level based on the visibility range compared to the ground truth at the column's bottom.

6. BENCHMARK FOR COMPARATIVE ANALYSIS

The purpose of various haze conditions is to proof the dehazing algorithm's efficiency; whether capable of removing haze in any hazy condition and preserving image quality. Based on VHAZE datasets, we have made the comparative analysis for the existing dehazing method, which is: Dark Channel Prior [14], Colour Attenuation Prior [18], DehazeNet [20], Haze-Line [21] and Multi-Layer Perceptron [35].

Table 5: The visual range and the corresponding weather condition and the scattering coefficient

Visibility Range, km	A dataset with actual distance map	A dataset with ground truth depth map
1 Dense haze		
2 Haze		
3 Haze		
4 Light haze		
Ground Truth		

7. IMAGE QUALITY ASSESSMENT

In this section, the dehazing methods applied to the synthesized haze image and evaluated with standard image quality assessment [36], which is the Mean-Squared Error (MSE), Peak-Signal to Noise Ratio (PSNR) in decibel (dB) unit and Structural Similarity Index Measurement (SSIM). Mean Squared Error is computed by averaging the squared intensity of the original image and the resultant image pixels as in

$$MSE = \frac{1}{NM} \sum_{m=0}^{M-1} \sum_{n=0}^{N-1} e(m, n)^2 \quad (4)$$

where $e(m, n)$ is the error difference between the original and the dehazed images. The lower the value of MSE, the lower the error. It is non-negative, and

values closer to zero are better. PSNR is a mathematical measure of image quality ratio between the original image and the dehazed image. The PSNR unit is in decibel (dB). PSNR is defined

Table 6: The comparison analysis of dehazing method used a dataset with the actual distance

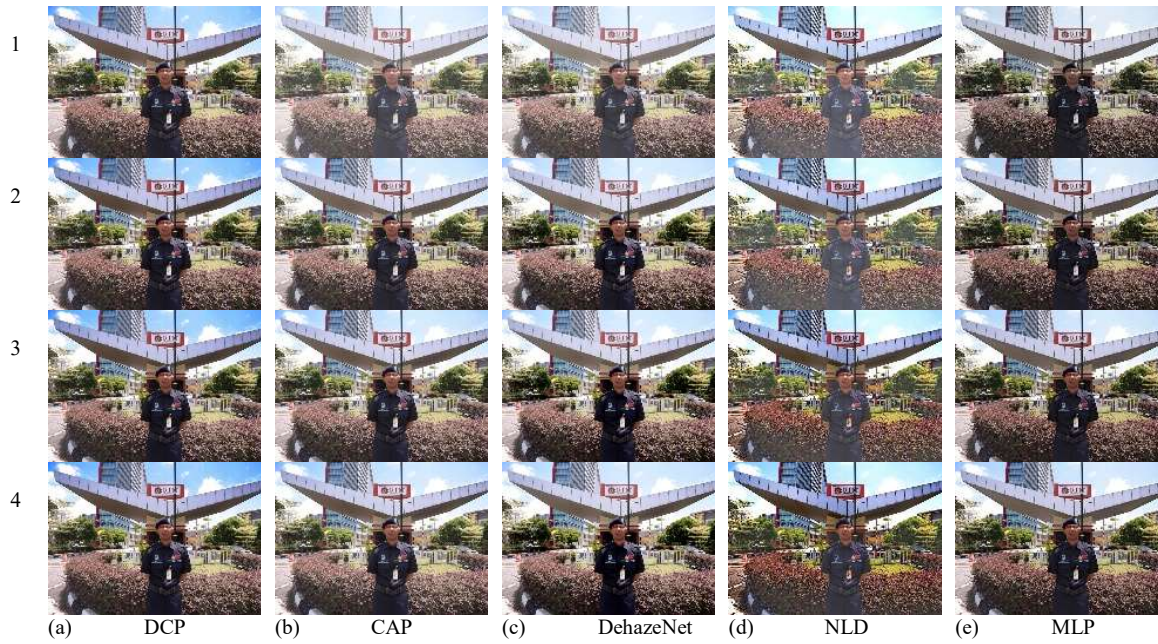
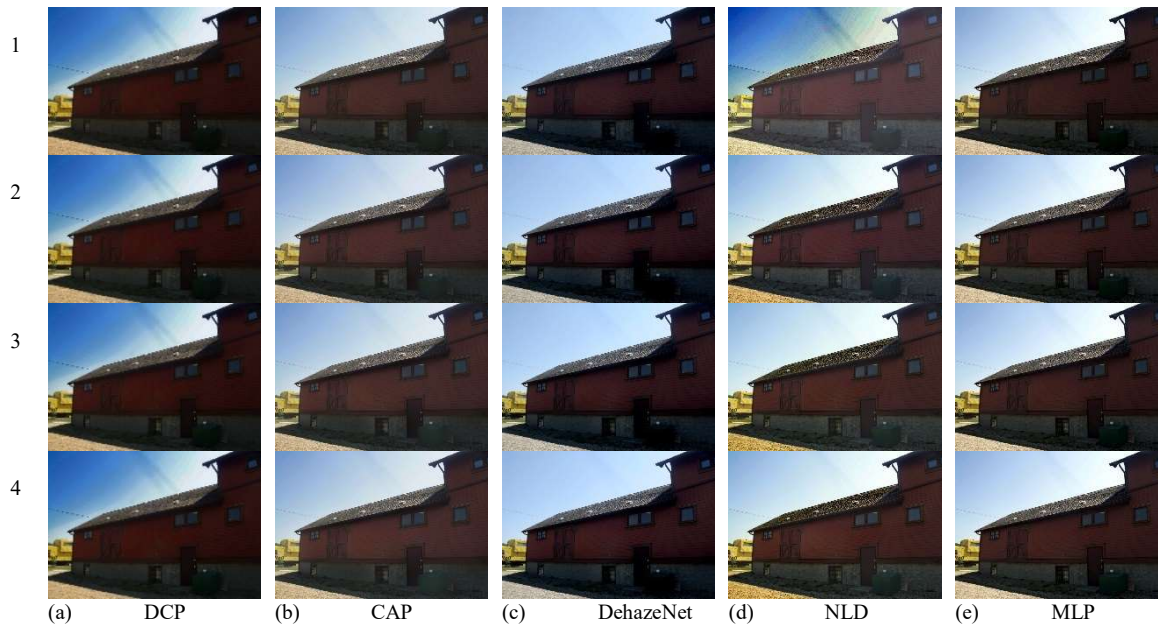


Table 7: The comparison analysis of dehazing method with dataset associated ground truth depth map



via the MSE. The MSE represents the cumulative squared error between the dehazed and the original image, whereas PSNR represents a peak error

measure. The higher the PSNR, the better the quality of the dehazed image. PSNR is defined as in

$$PSNR = 10 \log \frac{s^2}{MSE} \quad (5)$$

where $s=255$ for an 8-bit image.

SSIM is a method for measuring the similarity between two images. SSIM measures the quality of the image based on the original image as a reference. The SSIM formula is based on three comparison measurements between the samples of x and y : luminance(l), contrast (c) and structure(s) as in

$$S(x, y) = f(l(x, y), c(x, y), s(x, y)) \quad (6)$$

The resulting SSIM index is a decimal value between -1 and 1, and value one can only be reached in the case of two equivalent data sets, thus implying perfect structural similarity. No structural similarity is indicated by a value of 0.

Table 8: Evaluation for proposed haze dataset

km	IQA (dB)	DCP	CAP	DN	NLD	MLP
1	MSE	0.0071	0.0092	0.0035	0.0191	0.0056
	PSNR	21.5075	20.3531	24.5885	17.1888	22.4973
	SSIM	0.9230	0.9339	0.9663	0.8584	0.9540
2	MSE	0.0101	0.0018	0.0015	0.0199	0.0075
	PSNR	19.9742	27.3890	28.3691	17.0133	21.2236
	SSIM	0.9099	0.9751	0.9740	0.8541	0.9493
3	MSE	0.0111	0.0030	0.0034	0.0240	0.0076
	PSNR	19.5365	25.2879	24.6757	16.1977	21.2168
	SSIM	0.9042	0.9667	0.9342	0.8451	0.9449
4	MSE	0.0117	0.0038	0.0047	0.0307	0.0075
	PSNR	19.3360	24.1465	23.2813	15.1217	21.2335
	SSIM	0.9014	0.9590	0.9096	0.8282	0.9417

Table 9: Evaluation for HAZERD haze dataset

km	IQA (dB)	DCP	CAP	DN	NLD	MLP
1	MSE	0.0411	0.0085	0.0181	0.0277	0.0152
	PSNR	13.8649	20.6935	17.4194	15.5680	18.1945
	SSIM	0.5981	0.8745	0.6442	0.8030	0.7599
2	MSE	0.0406	0.0082	0.0192	0.0091	0.0135
	PSNR	13.9156	20.8878	17.1659	20.3957	18.6841

3	SSIM	0.6105	0.8905	0.6385	0.8892	0.7879
	MSE	0.0401	0.0076	0.0175	0.0105	0.0127
	PSNR	13.9653	21.2103	17.5664	19.7725	18.9783
	SSIM	0.6173	0.8996	0.6646	0.8798	0.8011
4	MSE	0.0398	0.0072	0.0173	0.0120	0.0120
	PSNR	14.0032	21.4392	17.6226	19.2239	19.2015
	SSIM	0.6220	0.9057	0.6707	0.8517	0.8102

Table 6 and Table 8 shows the result of dehazing methods assessed on our dataset with an actual distance map. The Dark Channel Prior method removed haze in all hazy conditions, but the sky region looks oversaturated. Colour Attenuation Prior efficient to reduce the haze at a light hazy condition and looks natural. However, it was not fully successes in dense haze conditions. Resultant images still have haze. For DehazeNet result, it seems perfect in removing the haze in all conditions and quality preservation specifically at dense haze conditions. But at the light hazy condition still was faced a disadvantage than CAP. The haze-Line method was a bad condition, where the result looks at enhancing contrast and unnatural in all conditions. For Multi-Layer Perceptron method, it made it useful to remove haze, but it seems to decrease the contrast of the image, which also became a bit darker.

Table 7 and Table 9 shows the image result of the dehazing method for a dataset with the ground truth depth map shown in Table 5. Although most of the dehazing methods can reduce haze in all hazy conditions, however, even in different image scenarios, the results highlight a uniform problem in dehazed images. DCP produces over-enhanced images, specifically in the sky region, in both situations. CAP and DehazeNet method look natural and similar to the original images. This result shows that the dehazing method was not very useful.

However, the limitation of this proposed dataset triggered on measure the accurate distance map for real images. The distance measurement could be inaccurate if use the random haze-free images due to unknown distance estimation. So, it requires a depth map measurement method. Thus, this propose only provide our haze-free image captured with a known distance. Besides, the simulation relied on four haze levels condition, it might not enough a volume of data to proof the dehazing's method efficiency. According to these

results, it shows that our proposed dataset which has four haze levels condition can be used for image dehazing algorithm. It might help to prove the efficiency of the dehazing approach if tested successfully at any haze level conditions.

8. CONCLUSION

A dehazing approach is advantageous and useful to many applications, including computer vision, surveillance systems and remote sensing. A great deal of effort has been made to dehaze to deliver the highest picture quality and achieve the goal of removing the haze. According to the observed limitations, there were the remaining problems which are not recovered to the dense haze or low haze [11,19,21] and brings the problems of haze level of thickness. This research emphasizes all haze levels of thickness issues.

This paper introduced a new dataset for hazy images and simulated the synthetic haze in a single image in four different hazy conditions based on the meteorological range. The importance of this experiment is to ensure the efficiency of the dehazing method to remove haze in different haze levels and to maintain the quality of the image. Therefore, a variety of standard dataset will produce better haze-free images that will be proved to be beneficial to other downstream application. This method will be increasingly studied in future research on different haze simulation condition and the provision of a dehazing algorithm that handles all the dehazing issues.

ACKNOWLEDGEMENT:

This research was funded by the Ministry of Higher Education through the Fundamental Research Grant Scheme and managed by the Research Management Centre (RMC) of University Technology Malaysia Vot No. R.K130000.7856.5F036.

REFERENCES:

- [1] S. G. Narasimhan and S. K. Nayar. Vision and the atmosphere. *International Journal of Computer Vision*, 48(3):233–254, 2002
- [2] Xue, R., Zhong, M., Zhang, E., Zhao, S., & Zhang, D. & Zhang, D.(2018, June). Real-time Image Haze Removal Method for Fire Scene Images. In 2018 6th International Conference on Machinery, Materials, and Computing Technology (ICMMCT 2018). Atlantis Press
- [3] Dong, T., Zhao, G., Wu, J., Ye, Y., & Shen, Y. (2019). Efficient Traffic Video Dehazing Using Adaptive Dark Channel Prior and Spatial-Temporal Correlations. *Sensors*, 19(7), 1593.
- [4] Koschmieder, “Theorie der horizontalen sichtweite,” in *Beitrage zur Physik der freien Atmosphere*, 1924.
- [5] F. Cozman, and E. Krotkov. Depth from scattering. In *Proceedings of IEEE Computer Society Conference on Computer Vision and Pattern Recognition*, pages 801–806, Jun 1997.
- [6] S. G. Narasimhan and SK. Nayar, “Contrast restoration of weather degraded images,” *IEEE Trans. on Pattern Analysis and Machine Intell.*, 2003.
- [7] Y. Y. Schechner, S. G. Narasimhan, and S. K. Nayar, “Polarization-based vision through the haze,” *Applied Optics*, 2003.
- [8] J. Kopf, B. Neubert, B. Chen, M. Cohen, D. Cohen-Or, O. Deussen, M. Uyttendaele, and D. Lischinski, “Deep photo: Model-based photograph enhancement and viewing,” in *Siggraph ASIA*, *ACM Trans. on Graph.*, 2008.
- [9] R. T. Tan, “Visibility in bad weather from a single image,” in *IEEE Intl. Conf. Comp. Vision and Pattern Recog. IEEE*, 2008, pp. 1–8.
- [10] R. Fattal, “Single image dehazing,” *ACM Trans. on Graphics*, vol. 27, no. 3, p. 72, 2008.
- [11] R. Fattal, “Dehazing using colour-lines,” *ACM Transaction on Graphics*, Vol. 34, no. 1, pp. 1–14, Nov. 2014.
- [12] J.-P. Tarel and N. Hautiere, “Fast visibility restoration from a single colour or grey level image,” in *IEEE Intl. Conf. Comp. Vision. IEEE*, 2009, pp. 2201–2208.
- [13] J.P. Tarel, N. Hautiere, L. Caraffa, A. Cord, H. Halmaoui, and D. Gruyer, “Vision enhancement in homogeneous and heterogeneous fog,” *IEEE Intelligent Transportation Systems Magazine*, Vol. 4, no. 2, pp. 6–20, Apr. 2012.
- [14] K. He, J. Sun, and X. Tang, “Single image haze removal using dark channel prior,” *IEEE Transaction on Pattern Analysis and Machine Intelligence*, Vol. 33, no. 12, pp. 1956–1963, Dec. 2011.
- [15] K. He, J. Sun, and X. Tang, “Guided image filtering,” in *IEEE Transactions on Pattern Analysis and Machine Intelligence (TPAMI)*, 2013.
- [16] G. Meng, Y. Wang, J. Duan, S. Xiang, and C. Pan, “Efficient image dehazing with boundary constraint and contextual regularization,” in *Proceedings of the IEEE International Conference Computer Vision*, Washington, DC, USA, 2013, pp. 617–624.

- [17] K. Tang, J. Yang, and J. Wang, "Investigating haze-relevant features in a learning framework for image dehazing," in Proceedings of the IEEE Conference Computer Vision Pattern Recognition, Columbus, Ohio, USA, 2014, pp. 2995–3002.
- [18] Q. Zhu, J. Mai, and L. Shao, "A fast single image haze removal algorithm using colour attenuation prior," *IEEE Transaction Image Processing*, Vol. 24, no. 11, pp. 3522–3533, Nov. 2015.
- [19] C. O. Ancuti and C. Ancuti, "Single image dehazing by multi-scale fusion," *IEEE Trans. Image Proc.*, vol. 22, no. 8, pp., 3271–3282, 2013.
- [20] B. Cai, X. Xu, K. Jia, C. Qing, and D. Tao, "Dehazenet: An end-to-end system for single image haze removal," *IEEE Transaction Image Processing.*, Vol. 25, no. 11, pp. 5187–5198, Nov. 2016.
- [21] D. Berman, T. Treibitz, and S. Avidan, "Non-local image dehazing," in Proceedings of the IEEE Conference Computer Vision and Pattern Recognition, Las Vegas, Nevada, USA, 2016, pp. 1674–1682.
- [22] C. Ancuti, C. O. Ancuti, and C. D. Vleeschouwer, "D-hazy: A dataset to evaluate quantitatively dehazing algorithms," in IEEE Intl. Conf. Image Proc., Sept 2016, pp. 2226–2230.
- [23] J. El Khoury, J.B. Thomas, A. Mansouri, "A Color Image Database for Haze Model and Dehazing Methods Evaluation," in Proceedings of the International Conference on Image and Signal Processing, Springer, Canada, 2016, pp. 109–117.
- [24] Y. Zhang, L. Ding, G. Sharma, "HazeRD: an outdoor dataset for dehazing algorithms," in Proceedings of the IEEE International Conference Image Processing, Beijing, China, 2017, pp. 3205–3209.
- [25] C. O. Ancuti, C. Ancuti, R. Timofte, and C. De Vleeschouwer. O-HAZE: a dehazing benchmark with real hazy and haze-free outdoor images. In *2018 IEEE/CVF Conference on Computer Vision and Pattern Recognition Workshops (CVPRW)*, 2018.
- [26] C. O. Ancuti, C. Ancuti, R. Timofte, and C. De Vleeschouwer. I-HAZE: a dehazing benchmark with real hazy and haze-free indoor images. In *arXiv:1804.05091*, 2018
- [27] <http://vision.middlebury.edu/stereo/data/scenes> 2014
- [28] <http://cs.nyu.edu/~silberman/datasets/nyudepthv2.html>
- [29] M. Sulami, I. Geltzer, R. Fattal, and M. Werman, "Automatic recovery of the atmospheric light in hazy images," in Proceedings of the IEEE International Conference Computational Photography, Santa Clara, California, USA, 2014, pp. 1–11.
- [30] Y. Bahat and M. Irani. Blind dehazing using internal patch recurrence. In *Proc. IEEE ICCP*, 2016.
- [31] D. Berman, T. Treibitz, and S. Avidan. Air-light estimation using haze-lines. In *Computational Photography (ICCP), 2017 IEEE International Conference on*, pages 1–9, 2017.
- [32] E. J. McCartney, "Optics of the atmosphere: scattering by molecules and particles," New York, John Wiley and Sons, Inc., 1976.
- [33] O'Neill, S. M., Lahm, P. W., Fitch, M. J., & Broughton, M. (2013). Summary and analysis of approaches linking visual range, PM_{2.5} concentrations, and air quality health impact indices for wildfires. *Journal of the Air & Waste Management Association*, 63(9), 1083–1090.
- [34] L. Ding and G. Sharma, "Fusing structure from motion and lidar for accurate dense depth map estimation," in IEEE Intl. Conf. Acoust., Speech, and Signal Proc., 2017, pp. 1283–1287.
- [35] Salazar-Colores, S., Cruz-Aceves, I., & Ramos-Arreguin, J. M. (2018). Single image dehazing using a multilayer perceptron. *Journal of Electronic Imaging*, 27(4), 043.
- [36] Z. Wang, A. C. Bovik, H. R. Sheikh, and E. P. Simoncelli, "Image quality assessment: from error visibility to structural similarity," *IEEE Trans. Image Processing*, vol. 13, no. 4, pp. 600–612, Apr. 2004.
- [37] Rad, A. E., Mohd Rahim, M. S., Kolivand, H., & Mat Amin, I. B. (2017). Morphological region-based initial contour algorithm for level set methods in image segmentation. *Multimedia Tools and Applications*, 76(2), 2185–2201. doi:10.1007/s11042-015-3196-y
- [38] Rakhmadi, A., Syazrah Othman, N. Z., Bade, A., Mohd Rahim, M. S., & Amin, I. M. (2010). Connected component labelling using components neighbours-scan labelling approach. *Journal of Computer Science*, 6(10), 1099–1107. doi:10.3844/jcssp.2010.1099.1107
- [39] Ruzinoor, C. M., Shariff, A. R. M., Pradhan, B., Rodzi Ahmad, M., & Rahim, M. S. M. (2012). A review on 3D terrain visualization of GIS data: Techniques and software. *Geo-Spatial*

Information Science, 15(2), 105-115.
doi:10.1080/10095020.2012.714101

- [40] Husain. N.A, Mohd Rahim. M.S, Kari. S, Chaudry. H (2020). "VRHAZE: The Simulation of Synthetic Haze Based on Visibility Range for Dehazing Method in Single Image". 6th International Conference on Interactive Digital Media (ICIDM 2020), 14th – 15th December 2020, International Virtual Conference.